



3D investigations of microscale mixing in helically coiled capillaries

Julia Schuler¹ · Jakob Herath¹ · Norbert Kockmann¹

Received: 16 December 2020 / Accepted: 25 March 2021 / Published online: 20 April 2021
© The Author(s) 2021

Abstract

In capillary reactors, improving radial mixing and narrowing the residence time distribution is of great importance for high selectivity and reaction performance. A well-known approach is inducing secondary flow patterns by coiling the capillary around a cylinder. To increase understanding of transport phenomena in helically coiled capillaries non-invasive 3D imaging approaches are required. In this perspective paper, we introduce X-ray-based micro-computed tomography for the investigation of dispersion of iodide in a helically coiled tube. The methodology presented here allows for the direct evaluation of radial concentration fields. By varying Dean number Dn and modified torsion parameter T^* , the effect of torsion and curvature on the radial concentration profile can be identified. Detailed knowledge of local radial mixing in helically coiled capillaries will help the precise prediction of reaction progress and selectivity.

Keywords Helically coiled capillary · Micro-computed tomography · Dean flow · Radial mixing · Capillary flow reactor · Local concentration fields

Introduction

In the context of process intensification in the chemical industry, performing processes in microfluidic devices is advantageous, especially for highly exothermic reactions, highly specialized products, or small production quantities. Continuous processes can be realized via laminar flow in simple straight capillaries. However, the flow profile is parabolic and radial mixing is solely governed by molecular diffusion [1]. Radial mixing can be improved by coiling the capillary. This approach is widely applied in the field of flow chemistry, as for the continuous production of nano-materials [2–6] or in viral inactivation reactors [7–9]. By coiling the capillary, a

centrifugal force is imposed on the parabolic flow profile leading to a secondary flow pattern. Therefore, the laminar flow profile is superimposed with two counter-rotating vortices normal to the main flow direction, the Dean vortices, which were first described by Dean [10, 11]. In a helically coiled tube (HCT) the two main parameters that affect the secondary flow pattern are curvature and torsion, represented by the non-dimensional Dean number Dn (Eq. (1)) [12–15] and the non-dimensional modified torsion parameter T^* (Eq. (2)) [15]. In Eqs. (1) and (2), Re is the Reynolds number, d_i and d_c are the inner diameter of the capillary and the coil diameter, and p is the pitch, see Fig. 3.

$$Dn = Re \cdot \sqrt{\frac{d_i}{d_c}} \quad (1)$$

$$T^* = \frac{Re \cdot \pi \cdot d_c}{p} \quad (2)$$

Increasing curvature, respectively Dn number, increases the intensity of Dean flow [16] and leads to improved radial mixing [12], a narrower residence time distribution (RTD) [17], and stabilization of the flow against turbulence [13, 18, 19]. Increasing torsion, which means decreasing the modified torsion parameter T^* , leads to destabilization of the flow against turbulences, reduction of the symmetry of the vortices, and broadening of the RTD [18–20].

Highlights

- Dispersion of iodide in water due to Dean vortices is investigated in a helically coiled tube.
- X-ray based micro-computed tomography is applied for the visualization of cross-sectional concentration fields.
- Increase in Dean number causes the formation of characteristic concentration field normal to the main flow direction.

✉ Julia Schuler
julia.schuler@tu-dortmund.de

¹ Laboratory of Equipment Design, Department of Biochemical and Chemical Engineering, TU Dortmund University, 44227 Dortmund, Germany

Investigating transport phenomena in helically coiled tubes is still of great interest [7, 8, 21–23]. Especially non-invasive imaging approaches promise great insights and are crucial for the validation of numerical simulations [24]. Flow profiles were already visualized in curved tubes using magnetic resonance imaging (MRI) [14, 25], digital holographic particle tracking velocimetry [12], and 2D and 3D particle image velocimetry (PIV) [24, 26–29]. In this perspective paper, X-ray micro-computed tomography (X- μ CT) is applied to visualize 3D concentration profiles of iodide (Γ) in an HCT. X- μ CT is non-invasive and offers high spatial resolutions without requiring optical access [30, 31]. Even though X-ray based computed tomography has already been successfully applied for the characterization of processes on a larger scale, among others [32–37], studies concerning its extension to the mini- or microscale are limited [31] and only very few studies concern the X-ray based investigation of mass transfer related problems [38–40]. Nonetheless, the proposed methodology offers great potential in gaining deeper knowledge about local radial mixing in HCTs, which is crucial for controlling reactions and their selectivity.

Results and discussion

Figure 1 shows resulting projection images and cross-sectional views of the FEP tube and the concentration field of Γ at angular positions of 0° , 360° , and 540° for different total volume flow rates and pitches. The angular positions are also marked in the projection images. In the cross-sectional slices, bright voxels indicate a high concentration of Γ and dark voxels indicate pure water.

It is visible from the cross-sectional voxel slices that the total liquid flow is divided into an iodide-rich and an iodide-poor region that are separated by a clear separation line. For an angular position of 0° , this separation line is horizontal for the lower volume flow rate, while it is inclined to the outside of the helix for the higher flow rate. The difference in the concentration fields resulting from V_1 and V_2 is likely to be caused by settling effects, as the KI solution (15w% KI, $\rho_s \approx 1173 \text{ kg m}^{-3}$) is known to have a higher density ($\Delta\rho_{rel} \approx 0.18$) than pure water. The residence time between the T-junction and the reference point of the helix (see Fig. 3) is significantly lower for the higher total volume flow rate V_2 . Here, the concentration profile at an angular position of 0° is still affected strongly by the first contact of the KI-rich liquid and the KI-poor liquid in the T-junction and the redirecting of the contacted liquids in the feed section. Between 0° and 360° the separation line becomes horizontal.

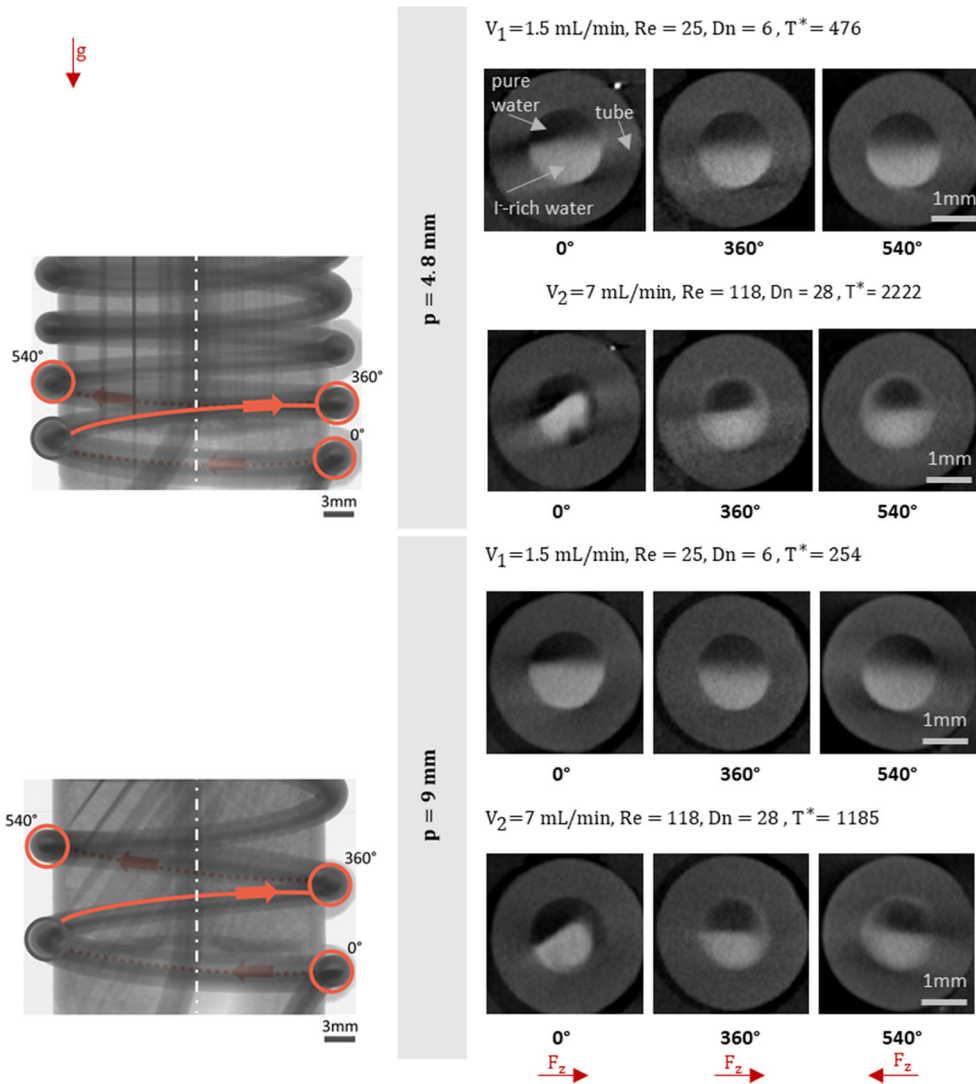
In the following, the effect of Re number on the Dean vortices, and hence the resulting radial concentration fields, is considered for $p_1 = 4.8 \text{ mm}$. For a given helix geometry, increasing

Re is realized by increasing the total volume flow rate V . Increasing Re simultaneously increases Dn and T^* . For the lower volume flow rate tested ($V_1 = 1.5 \text{ mL min}^{-1}$, $Re = 25$, $Dn = 6$, $T^* = 476$), Γ is transported upwards almost uniformly when following the main flow direction. Dean flow does not seem to be pronounced sufficiently to disturb the natural evolution of the concentration field due to diffusion. When increasing the total volume flow rate to $V_2 = 7 \text{ mL min}^{-1}$ ($Re = 118$, $Dn = 28$, and $T^* = 2222$) the concentration field significantly differs from the concentration field obtained for lower Re , Dn , and T^* . At an angular position of 360° , the concentration field shows the effect of the Dean vortices. The upper part of the tube cross-section predominantly contains pure water, but some Γ is entrained into the iodide-poor region of the cross-section, located at the tube wall. Furthermore, a higher Γ concentration can be found in the direction of the centrifugal force F_z . The same can be recognized inversely in the lower part of the tube cross-section for the iodide-rich phase and water. This characteristic concentration field is even pronounced stronger for an angular position of 540° . In total, better radial mixing can be observed for $V_2 = 7 \text{ mL min}^{-1}$ than for $V_1 = 1.5 \text{ mL min}^{-1}$ from the reconstructed cross-sectional views. This is especially true because the residence time for higher V in the shown number of turns is significantly reduced. Figure 2 gives a qualitative impression about the separation area between the iodide rich and the iodide poor region for p_1 along one turn of the helix starting at an angular position of 540° . For lower Re , the total fluid stream is clearly divided into the iodide rich region at the bottom and the iodide poor region at the top, both are clearly distinguished from each other by a nearly horizontal separation area. For the higher Re , a distinction can be made between the separation area between the iodide rich region and a region containing an intermediate concentration of iodide at the bottom (orange) and the separation area between the iodide poor region and the intermediate region at the top (blue). The difference between the appearances of the separation areas for different Re is contributed by the fact that Dean vortices are pronounced for higher Re .

The sole increase of the total volume flow rate is insufficient to distinguish between the influence of Dn and T^* on the resulting local concentration fields, as Dn and T^* both depend on Re . Different pitches, $p_1 = 4.8 \text{ mm}$ and $p_2 = 9 \text{ mm}$ are compared for the same total volume flow rates.

$V_1 = 1.5 \text{ mL min}^{-1}$ and $V_2 = 7 \text{ mL min}^{-1}$ to isolate the effect of T^* . For both Re tested, the cross-sectional concentration fields for p_1 are very similar to the concentration fields obtained with p_2 . However, at the higher volume flow rate ($V_2 = 7 \text{ mL min}^{-1}$) the concentration fields at 360° and 540° show slightly better mixing for p_1 than for p_2 with slightly more symmetrical concentration fields for the lower pitch. Additionally, it must be considered that for a higher pitch the total residence time within one turn is

Fig. 1 Left: Projection images (1944 × 1382) pixels for HCT with $p_1 = 4.8\text{ mm}$ and $p_2 = 9\text{ m}$. The orange lines indicate the main flow direction. Right: Cross-sectional views (180 × 180) voxels of capillaries with radial concentration field. Inside the tube, bright voxels indicate Γ -rich liquid, darker voxels indicate pure water. The red arrows indicate the direction of gravity g and centrifugal force F_z



longer, as is the tube distance. This supports the hypothesis that higher torsion from a larger pitch leads to reduced mixing. As the effect of T^* on the concentration fields is

apparently low, the strong dependence of Re on the concentration fields described previously originates from the effect of curvature (Dn).

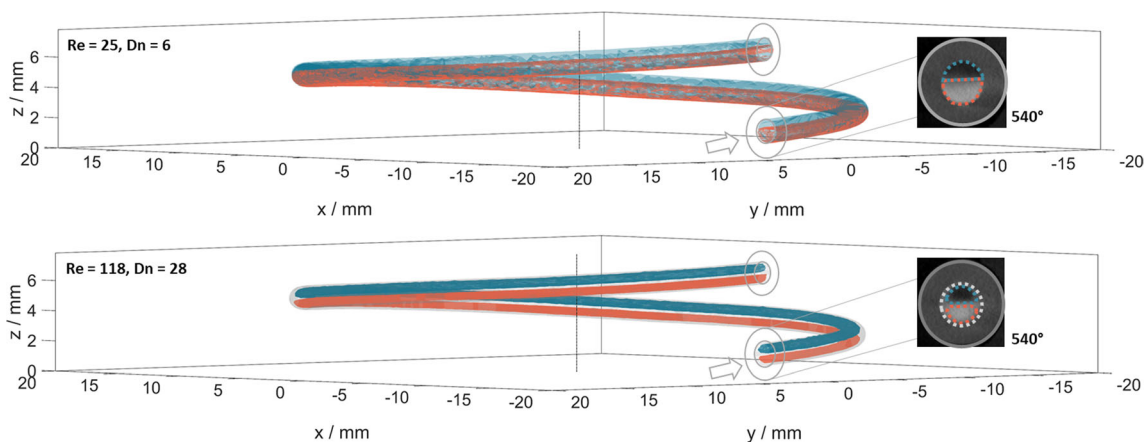


Fig. 2 Qualitative visualization of the separation area between iodide poor and iodide rich regions for different Dean numbers and p_1 extracted from the reconstructed CT-volume. The vertical line is the rotation axis of the helix. The size of the reconstructed voxel slices is (180 × 180) voxels

It can be concluded that both, torsion and curvature, affect the radial mixing in an HCT, as already reported in the literature [12, 13, 16–20]. Increasing curvature, represented by the Dean number, significantly increases radial mixing as the concentration field is affected by the secondary Dean flow pattern. Increasing torsion (decreasing T^*) for a fixed Dn number only slightly reduces the effect of Dean flow on radial mixing.

Experimental

The main objective of this perspective paper is to generate a defined radial concentration profile of an X-ray contrast agent in demineralized water whose disturbance can be observed due to the effect of Dean vortices. Potassium iodide is used as the contrast agent, which, when dissolved in water, forms K^+ and I^- ions. Both, K^+ and I^- , attenuate X-rays to a significantly higher level than pure water. Thereby, X-ray attenuation by I^- is higher than X-ray attenuation by K^+ , such that only the diffusion and dispersion of I^- can be registered in X-ray imaging [39]. The pure water and water containing 15 w% KI are contacted in a T-junction (IDEX Health & Science, IDEX Corporation, Northbrook, IL) that is connected to a helically coiled tube (HCT). The HCT consists out of a Fluorinated Ethylene Propylene (FEP) tube ($d_i = 1.58\text{mm}$, $d_o = 3.2\text{mm}$) that is coiled around a polylactide (PLA) support structure with a coil diameter ($d_c = 28.8\text{mm}$). To test the effect of torsion, the pitch of the HCT is varied ($p_1 = 4.8\text{mm}$, $p_2 = 9\text{mm}$). The HCT is mounted into a micro-computed tomography scanner (Bruker Skyscan 1275, RJL Micro & Analytic GmbH, Karlsdorf Neuthart, Germany) that is equipped with tubes for liquid supply and removal. The KI-rich mixture is pumped using a syringe pump (LAMBDA VIT-FIT by LAMBDA Instruments GmbH, Baar, Switzerland) and pure water is pumped using a high-pressure dosing pump (BlueShadow Pump 40P, KNAUER Wissenschaftliche Geräte GmbH, Berlin, Germany). Both pumps are placed outside the CT, see Fig. 3. Two different volume flow rates are tested, $V_1 = 1.5\text{mLmin}^{-1}$ and $V_2 = 7\text{mLmin}^{-1}$, resulting in Reynolds numbers of $Re_1 = 25$ and $Re_2 = 118$, Dean numbers of $Dn_1 = 6$ and $Dn_2 = 28$, and modified torsion numbers $254 < T^* < 2222$. The mean dynamic viscosity ($\bar{\eta} = 0.86\text{mPa}\cdot\text{s}$) for the calculation of Re is estimated according to data by Goldsack et al. [41]. The volume flow rate ratio of pure water and KI-rich water is 1. The total flow is monitored gravimetrically during the experiments. Scanning voltage is 43kV , the current is $190\mu\text{A}$, and exposure time is 30ms . The size of the resulting X-ray projection images is (1944×1382) pixels with pixel size = $18\mu\text{m} \times 18\mu\text{m}$.

During image acquisition, X-ray projection images are acquired for different angular positions. The resulting set of projection images is reconstructed to a 3D dataset using the

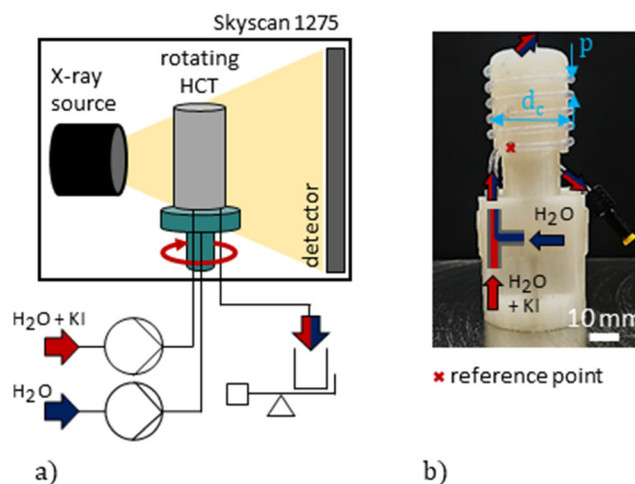


Fig. 3 **a** Schematic of the experimental set-up. Pure water and pure water enriched with potassium iodide (KI) are pumped into the rotating helically coiled tube (HCT) that is mounted into the computed tomography scanner (Skyscan 1275). The total volume flow rate is measured at the outlet gravimetrically. **b** Photograph of HCT and schematic of the contacting device (T-junction). Pure water is fed from the side inlet and KI-rich water from the bottom inlet

reconstruction software NRecon (Bruker, Billerica, MA). The 3D data set consists of a stack of cross-sectional slices, each of which is composed of voxels, the 3D equivalent of pixels. The total size of the 3D image is $(1944 \times 1944 \times 1382)$ voxels with voxel size = $18\mu\text{m} \times 18\mu\text{m} \times 18\mu\text{m}$. The reconstructed CT-volume is used to extract the qualitative separation areas between iodide rich, intermediate, and iodide poor region of the total fluid stream.

Summary and outlook

In this perspective paper, micro-computed tomography was successfully applied for the visualization of the concentration field of iodide in helically coiled tubes (HCT). The effect of curvature and torsion on radial mixing was studied by varying the total volume flow rate and the pitch. It was found that increasing Dn number leads to the formation of a characteristic concentration profile and enhanced radial mixing. At the same time, increasing the pitch reduces radial mixing due to Dean vortices only slightly. The presented methodology offers high potential and will therefore be systematically extended. The current investigations will be enriched with further post-processing of reconstructed voxel slices to obtain concentration profiles and robust quantitative statements about mixing quality. Additionally, more flow conditions will be tested and the effect of different liquid densities on radial mixing must be addressed in more detail. The proposed method will not only help the fundamental understanding of dispersion in HCT but also in diverse forms of passive microreactors. It can even be extended to the investigation of certain reactions, such as

precipitation reactions. Finally, concentration fields obtained with the presented methodology will help in validating numerical simulations that aim to simulate and optimize microreactors with internal convective mixing.

Notation d_c , coil diameter [m]; d_i , inner tube diameter [m]; d_o , outer tube diameter [m]; $\Delta\rho_{rel}$, relative density difference between KI solution and water [-]; F_z , centrifugal force [N]; g , gravity constant [m s^{-2}]; Dn , Dean number [-]; p , pitch [m]; ρ_s , density of KI solution [kg m^{-3}]; Re , Reynolds number [-]; T^* , modified torsion parameter [-]; V , volume flow rate [$\text{m}^3 \text{s}^{-1}$]

Acknowledgements We would like to thank RJI Micro & Analytic, Karlsdorf-Neuthard, Germany, for technical support and training. Furthermore, we would like to acknowledge C. Schrömgies (Laboratory of Equipment Design, TU Dortmund University, Germany) for technical advice.

Funding Open Access funding enabled and organized by Projekt DEAL. The Bruker Skyscan 1275 was funded by the German Research Foundation (DFG, grant number INST 212/397-1). General funding is provided by TU Dortmund University, Germany.

Data availability Not applicable.

Code availability Not applicable.

Declarations

Conflicts of interest/Competing interests On behalf of all authors, the corresponding author states that there is no conflict of interest.

Open Access This article is licensed under a Creative Commons Attribution 4.0 International License, which permits use, sharing, adaptation, distribution and reproduction in any medium or format, as long as you give appropriate credit to the original author(s) and the source, provide a link to the Creative Commons licence, and indicate if changes were made. The images or other third party material in this article are included in the article's Creative Commons licence, unless indicated otherwise in a credit line to the material. If material is not included in the article's Creative Commons licence and your intended use is not permitted by statutory regulation or exceeds the permitted use, you will need to obtain permission directly from the copyright holder. To view a copy of this licence, visit <http://creativecommons.org/licenses/by/4.0/>.

References

- Abushammala O, Hreiz R, Lemaître C et al (2020) Optimal design of helical heat/mass exchangers under laminar flow: CFD investigation and correlations for maximal transfer efficiency and process intensification performances. *Int J Heat Mass Transf* 153:119610. <https://doi.org/10.1016/j.ijheatmasstransfer.2020.119610>
- Pinho B, Torrente-Murciano L (2020) Continuous manufacturing of silver nanoparticles between 5 and 80 nm with rapid online optical size and shape evaluation. *React Chem Eng* 5:342–355. <https://doi.org/10.1039/C9RE00452A>
- Besenhard MO, LaGrow AP, Famiani S et al (2020) Continuous production of iron oxide nanoparticles via fast and economical high temperature synthesis. *React Chem Eng* 5:1474–1483. <https://doi.org/10.1039/D0RE00078G>
- Epps RW, Volk AA, Abdel-Latif K et al (2020) An automated flow chemistry platform to decouple mixing and reaction times. *React Chem Eng* 5:1212–1217. <https://doi.org/10.1039/D0RE00129E>
- Besenhard MO, LaGrow AP, Hodzic A et al (2020) Coprecipitation synthesis of stable iron oxide nanoparticles with NaOH: New insights and continuous production via flow chemistry. *Chem Eng J* 399:125740. <https://doi.org/10.1016/j.cej.2020.125740>
- Epps RW, Bowen MS, Volk AA et al (2020) Artificial chemist: an autonomous quantum dot synthesis bot. *Adv Mater* 32:e2001626. <https://doi.org/10.1002/adma.202001626>
- Amarikwa L, Orozco R, Brown M et al (2019) Impact of dean vortices on the integrity testing of a continuous viral inactivation reactor. *Biotechnol J* 14:e1700726. <https://doi.org/10.1002/biot.201700726>
- Brown MR, Orozco R, Coffman J (2020) Leveraging flow mechanics to determine critical process and scaling parameters in a continuous viral inactivation reactor. *Biotechnol Bioeng* 117:637–645. <https://doi.org/10.1002/bit.27223>
- Parker SA, Amarikwa L, Vehar K et al (2018) Design of a novel continuous flow reactor for low pH viral inactivation. *Biotechnol Bioeng* 115:606–616. <https://doi.org/10.1002/bit.26497>
- Dean WR (1928) LXXII. The stream-line motion of fluid in a curved pipe (Second paper). The stream-line motion of fluid in a curved pipe (Second paper). *Lond Edinb Phil Mag J Sci* 5:673–695. <https://doi.org/10.1080/14786440408564513>
- Dean WR (1927) XVI. Note on the motion of fluid in a curved pipe. *Lond Edinb Phil Mag J Sci* 4:208–223. <https://doi.org/10.1080/14786440708564324>
- Kim S, Lee SJ (2009) Measurement of Dean flow in a curved micro-tube using micro digital holographic particle tracking velocimetry. *Exp Fluids* 46:255–264. <https://doi.org/10.1007/s00348-008-0555-8>
- Manlapaz RL, Churchill SW (1980) Fully developed laminar flow in a helically coiled tube of finite pitch. *Chem Eng Commun* 7:57–78. <https://doi.org/10.1080/00986448008912549>
- Mejia Mendez DL, Lemaître C, Castel C et al (2017) Membrane contactors for process intensification of gas absorption into physical solvents: Impact of dean vortices. *J Membr Sci* 530:20–32. <https://doi.org/10.1016/j.memsci.2017.02.016>
- Klutz S, Kurt SK, Lobedann M et al (2015) Narrow residence time distribution in tubular reactor concept for Reynolds number range of 10–100. *Chem Eng Res Des* 95:22–33. <https://doi.org/10.1016/j.cherd.2015.01.003>
- Litster S, Pharoah JG, Djilali N (2006) Convective mass transfer in helical pipes: effect of curvature and torsion. *Heat Mass Transf* 42:387–397. <https://doi.org/10.1007/s00231-005-0029-y>
- Nigam KDP, Vasudeva K (1980) Residence time distribution in static mixer. *Can J Chem Eng* 58:543–544. <https://doi.org/10.1002/cjce.5450580421>
- Cioncolini A, Santini L (2006) An experimental investigation regarding the laminar to turbulent flow transition in helically coiled pipes. *Exp Therm Fluid Sci* 30:367–380. <https://doi.org/10.1016/j.expthermflusci.2005.08.005>
- Yamamoto K, Akita T, Ikeuchi H et al (1995) Experimental study of the flow in a helical circular tube. *Fluid Dyn Res* 16:237–249. [https://doi.org/10.1016/0169-5983\(95\)00022-6](https://doi.org/10.1016/0169-5983(95)00022-6)
- Saxena AK, Nigam KDP (1983) Effect of coil pitch and cross-sectional ellipticity on RTD for diffusion-free laminar flow in coiled tubes. *Chem Eng Commun* 23:277–289. <https://doi.org/10.1080/00986448308940479>
- Pal SK, Dhasmana P, Nigam KDP et al (2020) Tuning of particle size in a helical coil reactor. *Ind Eng Chem Res* 59:3962–3971. <https://doi.org/10.1021/acs.iecr.9b04774>

22. Junqua R, Vinsonneau E, Ghidossi R (2020) Microbial stabilization of grape musts and wines using coiled UV-C reactor. *OENO One* 54. <https://doi.org/10.20870/oeno-one.2020.54.1.2944>
23. Mendez DLM, Castel C, Lemaitre C et al (2019) Improved performances of vacuum membrane distillation for desalination applications: Materials vs process engineering potentialities. *Desalination* 452:208–218. <https://doi.org/10.1016/j.desal.2018.11.012>
24. Kováts P, Martins FJWA, Mansour M et al (2020) Tomographic PIV measurements and RANS simulations of secondary flows inside a horizontally positioned helically coiled tube. *Exp Fluids* 61. <https://doi.org/10.1007/s00348-020-02950-6>
25. Bulusu KV, Plesniak MW (2018) Insights on arterial secondary flow structures and vortex dynamics gained using the MRV technique. *Int J Heat Fluid Flow* 73:143–153. <https://doi.org/10.1016/j.ijheatfluidflow.2018.08.002>
26. Brito M, Sanches P, Ferreira RML et al (2017) Experimental study of the transient flow in a coiled pipe using PIV. *J Hydraul Eng* 143: 4016087. [https://doi.org/10.1061/\(ASCE\)HY.1943-7900.0001253](https://doi.org/10.1061/(ASCE)HY.1943-7900.0001253)
27. Jain A, Ewing D, Ching CY (2019) Time-resolved refractive index matched PIV measurements inside and downstream of a 90° bend. *Exp Therm Fluid Sci* 107:88–106. <https://doi.org/10.1016/j.exptthermfluidsci.2019.05.007>
28. Li Y, Wang X, Zhou B et al (2017) Dean instability and secondary flow structure in curved rectangular ducts. *Int J Heat Fluid Flow* 68: 189–202. <https://doi.org/10.1016/j.ijheatfluidflow.2017.10.011>
29. Kalpakli Vester A, Sattarzadeh SS, Örlü R (2016) Combined hot-wire and PIV measurements of a swirling turbulent flow at the exit of a 90° pipe bend. *J Vis* 19:261–273. <https://doi.org/10.1007/s12650-015-0310-1>
30. Schuler J, Kockmann N (2020) Micro-computed tomography for the investigation of stationary liquid–liquid and liquid–gas interfaces in capillaries. *AIChE J* 66. <https://doi.org/10.1002/aic.16890>
31. Schuler J, Neuendorf LM, Petersen K et al (2020) Micro-computed tomography for the 3D time-resolved investigation of monodisperse droplet generation in a co-flow setup. *AIChE J*. <https://doi.org/10.1002/aic.17111>
32. Azizi S, Yadav A, Lau YM et al (2017) On the experimental investigation of gas–liquid flow in bubble columns using ultrafast X-ray tomography and radioactive particle tracking. *Chem Eng Sci* 170: 320–331. <https://doi.org/10.1016/j.ces.2017.02.015>
33. Bieberle M, Barthel F, Hampel U (2012) Ultrafast X-ray computed tomography for the analysis of gas–solid fluidized beds. *Chem Eng J* 189–190:356–363. <https://doi.org/10.1016/j.cej.2012.02.028>
34. Große Daldrup A, Crine M, Marchot P et al (2019) An approach to separation efficiency modelling of structured packings based on X-ray tomography measurements: Application to aqueous viscous systems. *Chem Eng Sci* 204:310–319. <https://doi.org/10.1016/j.ces.2019.03.059>
35. Lau YM, Möller F, Hampel U et al (2018) Ultrafast X-ray tomographic imaging of multiphase flow in bubble columns – Part 2: Characterisation of bubbles in the dense regime. *Int J Multiphase Flow* 104:272–285. <https://doi.org/10.1016/j.ijmultiphaseflow.2018.02.009>
36. Schug S, Arlt W (2016) Imaging of fluid dynamics in a structured packing using X-ray computed tomography. *Chem Eng Technol* 39:1561–1569. <https://doi.org/10.1002/ceat.201600278>
37. Toye D, Marchot P, Crine M et al (1998) Local measurements of void fraction and liquid holdup in packed columns using X-ray computed tomography. *Chem Eng Process Process Intensif* 37: 511–520. [https://doi.org/10.1016/S0255-2701\(98\)00058-0](https://doi.org/10.1016/S0255-2701(98)00058-0)
38. Keshmiri K, Pourmohammadbagher M, Huang H et al (2019) Microfluidics to determine the diffusive mass transfer of a low viscosity solvent into a high viscosity hydrocarbon. *Fuel* 235: 1327–1336. <https://doi.org/10.1016/j.fuel.2018.08.108>
39. Nakashima Y (2000) The use of X-ray CT to measure diffusion coefficients of heavy ions in water-saturated porous media. *Eng Geol* 56:11–17. [https://doi.org/10.1016/S0013-7952\(99\)00130-1](https://doi.org/10.1016/S0013-7952(99)00130-1)
40. Boden S, Haghnegahdar M, Hampel U (2017) Measurement of Taylor bubble shape in square channel by microfocus X-ray computed tomography for investigation of mass transfer. *Flow Meas Instrum* 53:49–55. <https://doi.org/10.1016/j.flowmeasinst.2016.06.004>
41. Goldsack DE, Franchetto R (1977) The viscosity of concentrated electrolyte solutions. I. Concentration dependence at fixed temperature. *Can J Chem* 55:1062–1072. <https://doi.org/10.1139/v77-148>

Publisher's note Springer Nature remains neutral with regard to jurisdictional claims in published maps and institutional affiliations.

Julia Schuler studied Mechanical Engineering at the Paderborn University. In July 2018, she started her work as a research assistant at the Laboratory of Equipment Design, TU Dortmund University, Germany. Her focus is on the experimental investigation of single- and multiphase transport phenomena in capillaries with micro computed tomography.

Jakob Herath studied Chemical Engineering at TU Dortmund University since 2013. He graduated with the master thesis “Investigation of passive and laminar mixing in straight and coiled capillaries using X-ray computed microtomography” at the Laboratory of Equipment Design in 2021.

Norbert Kockmann studied mechanical engineering at the Technical University of Munich and completed his Dr.-Ing. in process engineering at the University in Bremen. After 5 years in chemical industry as project manager he joined Freiburg University, IMTEK in 2001 as group leader for micro process engineering. In 2007, Dr. Kockmann joined Lonza Ltd., Visp, Switzerland, as senior scientist responsible for continuous flow processes and microreactor technology. In April 2011, Norbert Kockmann was appointed as full professor for Equipment Design at TU Dortmund University, Germany. His research interests are on small-scale device for continuous chemical processes, modular design, and process intensification. His work includes fundamental investigations of small-scale multiphase flow, modelling and simulation accompanied by modern sensing technology and machine-learning methods.